Electrochimica Acta 499 (2024) 144675



Contents lists available at ScienceDirect

Electrochimica Acta

journal homepage: www.journals.elsevier.com/electrochimica-acta





Electrical modeling of an electrochemical sensor operating at the redox cycling mode

Tali Dotan [b], Aakash Jog [c], Yosi Shacham-Diamand [a,*]

[a] Scojen Institute for Synthetic Biology, Reichman University, Herzliya, Israel
[b] Department of Chemical Engineering, Massachusetts Institute of Technology, Cambridge, Massachusettes 02139, United States of America
[c] School of Electrical Engineering, Tel Aviv University, Tel Aviv, Israel

ARTICLE INFO

Keywords:
Redox cycling
Interdigitated electrode array
Impedance spectroscopy

ABSTRACT

In this work, the direct current vs. voltage (DC) characteristics, and the alternate current (AC) impedance of a 1D four-electrode electrochemical cell, operating under redox-cycling conditions, are presented and discussed. The analysis refers to a four-electrode electrochemical system with one positively biased working electrode, one negatively biased working electrode, one auxiliary electrode, and one reference electrode operating in a redox cycling mode. This configuration is useful, for example, for electrochemical biosensors that can benefit from the inherent redox-cycling amplification of the apparatus. An aqueous buffered electrolyte is assumed, containing electrochemically active species that can be oxidized on the anode, with a positive overpotential. Meanwhile, the product of the oxidation reaction can diffuse to the other working electrode which has a negative overpotential, where the product is reduced. The analysis in this paper assumes that oxidation is the dominant mechanism at the anode, reduction is the dominant mechanism at the cathode, and the transport between them is dominated by diffusion. Since it is a 1D model, an ideal lossless redox cycling, i.e. both working electrodes' currents (anodic and cathodic) are of the same magnitude with opposite signs, is assumed. Next, the small signal (AC) impedance of the electrochemical cell was calculated assuming that the AC signal modifies the oxidation reaction rate at the anode while the reduction reaction rate at the cathode is fixed. The impedance under redox cycling is calculated vs. frequency for various oxidation and reduction rates and both Bodé and Nyquist plots of the impedance are presented. The last part of the paper presents measured data for both DC and AC (i.e. Bodé and Nyquist plots) experiments with interdigitated array (IDA) electrodes, 5 & 10 μm spacing, operating under redox cycling conditions. The DC measurements were conducted in a 6 mM ferricyanide [$K_3Fe(CN)_6$] in 0.1 M Phosphate Buffer Saline (PBS) solution, pH 7.4. The AC measurements were conducted in 10 mM & 100 nM ferricyanide ($K_3Fe(CN)_6$) in 100 mM KNO_3 aqueous electrolyte. A critical discussion follows the results section where the highlights and problems of the models are discussed.

1. Introduction

In this paper, we present both DC (direct current) and AC (alternating current) modeling of an electrochemical cell, with two working electrodes biased in opposite potentials. This configuration allows redox cycling of molecules or ions that can be reduced on one electrode, and the product can be transported and oxidized on the other electrode and converted to the original species. Such devices have been used for numerous applications, one of them is for biosensing [1–3]. Using redox-cycling is attractive to biosensing since it offers on-chip amplification, improving signal level [4]. This was demonstrated for example for DNA sensors [5], and immunosensors [6]. Redox cycling can be found in numerous variations; for example, conventional [7–9] sensors, integrated with microfluidics [10–12], in an "in-vivo two-way" system using whole-cell bidirectional electron transfer" (e.g. without a second electrode, with two different molecules [13]), and in "in vivo" functional plant-based bio-electrochemical sensors [14].

This paper focuses on devices with electrolyte systems that are similar to those in electrochemical biosensors, i.e. with moderate pH buffer solutions working under relatively low to moderate current densities. Hence, no high current or high concentration effects are under consideration.

* Corresponding author.
E-mail address: yosish@eng.tau.ac.il (Y. Shacham-Diamand).

https://doi.org/10.1016/j.electacta.2024.144675
Received 15 April 2024; Accepted 2 July 2024
Available online 10 July 2024
0013-4686/© 2024 Elsevier Ltd. All rights are reserved, including those for text and data mining, AI training, and similar technologies.

We assume a four-electrode system where there is also a counter electrode and a reference or a quasi-reference electrode. We take into consideration both the transport effect (e.g. diffusion) of the two species and the electrochemical reduction/oxidation rates at the electrodes. The AC modeling assumes a small signal applied to one of the working electrodes (Fig. 1, W2) while the other one (Fig. 1, W1) is at fixed bias. This implies unique boundary conditions at the two electrodes following the laws of conservation of charge and conservation of mass. Ideal conditions are assumed where each molecule (or ion) that is reduced (or oxidized) at one of the working electrodes, generates another molecule (or ion) that can be oxidized (or reduced) at the other working electrode. Assuming a 1st order oxidation and reduction reactions the electrochemical current is proportional to the concentrations of the species at the electrodes multiplied by the reaction rates:

$$I \propto k \cdot C(\textit{at the electrodes}) \tag{1}$$

The concentration units in this manuscript are $[cm^{-3}]$, the reaction rates' units are $[cm/sec]$ and $k \cdot C$ is the flux of the species towards or from the electrodes with units of $[cm^{-2} \cdot sec^{-1}]$. Under DC-only conditions (at W1) the reaction rate, k, is fixed. However, the concertation still can fluctuate. Therefore, the AC flux on the fixed bias electrode is not necessarily zero; Therefore, there is a possibility of an AC component for the diffusion flux even at the DC-biased electrode. This generates a "back-flow" of species out of that electrode with the same amplitude as the species arriving at the electrode but with an opposite phase. The "backflow" species diffuse to the other electrode (W2) where there is an AC component for the bias excitation that determines the boundary condition there. Under very large reaction rates, i.e. under high overpotentials, the AC fluctuations become very small, and the solution reaches asymptotic values that can be modeled by a (relatively compared to the full model) simple approximation. A detailed discussion related to the effect of the reaction rates is presented in this paper, starting from the regime where there is no redox cycling to the regime with fully developed redox cycling.

In a conventional three-electrode electrochemical cell, the oxidation/reduction reactions are associated with the transfer of a finite number of electrons to or from the electrolyte depending on the valence of the oxidant/reductant species. Therefore, the immediate current after applying a bias neglecting transport effects, is a function of the potential difference between the working electrode and the reference electrode. In a redox-cycling-based four-electrode electrochemical cell, the products of the reactions on the two electrodes are recycled, contributing another electron at each cycle to the cell current. This process can continue therefore, every molecule (or ion) under redox cycling conditions contributes more electrons compared to the single working electrode cell.

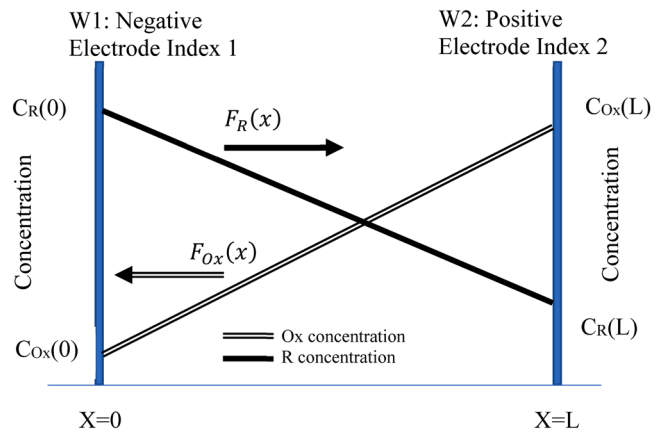


Fig. 1. Schematic sketch of the electrodes' positions and the ions (or molecules) concentration at a steady state. The subtitles "Ox" and "R" refer to oxidized and reduced states, respectively.

Therefore, the typical current/voltage characteristics of a 4-electrode cell under redox cycling exhibit a higher maximum current, than a 3-electrode cell. This is also known as redox-cycling amplification.

In the theoretical part of this paper, we look at the case where the reducing electrode is kept at a fixed negative bias where reducing is dominant while the potential of the oxidizing electrode is varied. The same analysis will be valid in the opposite case where the oxidizing electrode is kept at a fixed positive bias where the oxidizing reaction is dominant while the potential of the reducing electrode is varied.

In the case where the potential of the oxidizing electrode is varied, three regimes of operation can be defined where there are: 1. no redox cycling, 2. strong redox cycling, and 3. weaker redox cycling compared to the 2nd regime (A transition region). When the potentials at the oxidizing and reducing electrodes enable redox cycling, the current is derived from the electrode's electrochemical surface reactions while being limited by the transport effects between the electrodes (i.e., diffusion and convection). In this paper, we treat the case where there is no fluid flow, i.e. no convection.

Redox cycling has been discussed in numerous papers. One of the first papers to analyze this phenomenon is the work by Anderson and Reilley from 1965 [15]. They refer to it as "Thin layer electrochemistry". This name represents the essence of this effect which emerges from the situation where two working electrodes, under different bias conditions, are close enough to introduce cross-coupling effects. They cite a few other papers by Christensen et al. [16,17], Hubbard et al. [18] and Oglesby et al. [19], which all discuss the issue of "thin-layer electrochemistry".

The paper of Anderson and Reilley [15] describes the Redox Amplification phenomena and provides a simple solution for the steady state conditions. In their analysis, since the electrolyte is very thin, they assume a 1D model where the total number of oxidants (N_{0x}) and reductants (N_R) is fixed:

$$N_{0x} + N_R = N_T \tag{2}$$

At steady state, we assume that the concentrations are a linear function of the distance, and the fluxes of the oxidants (F_{Ox}) and that of the reductant (F_R) are constant over the sample (Fig. 1).

The following analysis can be applied to an arbitrary initial concertation. However, we will follow the same route as Anderson and Reilley [15] who assumed that the initial amount of the oxidant (Ox) is N_T and that of the reductant (R) is zero. It is assumed that at the coordinate $x = 0$, the electrode is negatively biased, so the species marked as "Ox" are reduced, while at the coordinate $x = L$ the electrode is positively biased, so the species marked as "R" are oxidized. Both reactions can be written as: (following the notation by Vivier, V. and Orazem, [25]):

$$Ox + ne^- \underset{k_{ox}}{\overset{k_r}{\rightleftharpoons}} R \tag{3}$$

Where n is the number of electrons transferred. k_r is the reduction reaction rate of the oxidant species (species with the index "ox") at the negative electrode while k_{ox} is the oxidation rate of the reductant species (with the index "r") on the positive electrode.

The reaction rates on a given electrode depend on the overpotential drop on that electrode:

$$k_{ox} = k_{ox,0} \cdot e^{\frac{qn\alpha}{kT} \cdot \eta} \;\&\; k_r = k_{r,0} \cdot e^{-\frac{qn(1-\alpha)}{kT} \cdot \eta} \tag{4}$$

Where $\eta = E - E^0$ is the overpotential [20], E^0 is the electrochemical redox potential of that reaction as given by the Nernst law [20], q is the electron charge, k is the Boltzmann constant, α is a symmetry factor, and T is the temperature. Note that the electrochemical redox potential is slightly different from the potential at steady state, as explained by the derivation of the Butler-Volmer equation [20]. An alternative way to write the reaction rates appears in the paper of Vivier and Orazem, [25]:

$$k_{ox} = k_{ox,0}\cdot e^{b_a\cdot V} \text{ and } k_r = k_{r,0}\cdot e^{-b_c\cdot V} \quad (5)$$

Where $b_a = \frac{qn\alpha}{kT}$ and $b_c = \frac{qn(1-\alpha)}{kT}$. The voltage V is the same over-potential η that has been defined before. Using this notation, the Faradic current of each electrode can be written, assuming a 1D model for an electrode with an area A, as:

$$I_F = \left[K_{ox,0}\cdot e^{b_a\cdot V}\cdot C_r(x_e,t) - K_{r,0}\cdot e^{-b_c\cdot V}\cdot C_{ox}(x_e,t)\right] \quad (6)$$

Where x_e is the coordinate of the electrode, $K_{ox,0} = qnAk_{ox}$ and $K_{r,0} = qnAk_r$. Also, in this manuscript $x_e \equiv x_c = 0$ for the cathode (negative electrode) and $x_e \equiv x_a = L$ for the anode (Positive electrode).

Note that this paper deals with electrochemical cells with two working electrodes, therefore, there will be two sets of indices. We assigned the sub-index "1″ for the negative electrode, where there is the reduction, and the sub-index "2″ for the positive electrode where there is oxidation. This notation was selected to avoid confusion with the indices *a* and *c* chosen for the anode and the cathode in reference [25] that are used to assign the indices for oxidation and reduction on the same electrode.

The redox cycling model assumes ideal conditions where under a steady state, the same number of electrons is being transferred over both electrodes. This is an idealization of the system which is justified since it highlights the effect of redox cycling and explains most of the effects that are being measured in a real device. Note that in most "real-life" situations, the electrochemical biosensor also contains species that do not participate in the redox cycling. Therefore, we can get currents that can be due to "only oxidation" at the anode, or "only reduction" at the cathode in addition to the currents of the redox cycling where the same species experience both reduction and oxidation. Hence, they can maintain a fixed DC current while "shuttling" electrons from the cathode to the anode. This current occurs when the concentration of the reductants R is zero at $x = L$ and the concentration of the oxidants Ox is zero at $x = 0$. In that case, the limiting current, i_{ss}^{lim}, at steady-state under high enough over-potentials at both oxidizing (index "2″) and reducing (index "1″) electrodes (*i.e.* $\eta_{ox,2}, -\eta_{r,1} \gg \frac{kT}{q}$), where the current is diffusion limited, is calculated by [1]:

$$i_{ss}^{lim} = qnAD_R\cdot\frac{\left(C_R^{ss}\right)_{x=0}}{L} = qnAD_{0x}\cdot\frac{\left(C_{Ox}^{ss}\right)_{x=L}}{L} \quad (7)$$

Where D_R and D_{0x} are the diffusion coefficients of R and Ox, respectively, $\left(C_R^{ss}\right)_{x=0}$ is the concentration of R under steady state at $x = 0$ and $\left(C_{ox}^{ss}\right)_{x=L}$ is the concentration of Ox under a steady state at $x = L$. Using the mass conservation law (eqn. 1) they showed that the limiting current is given by:

$$i_{ss}^{lim} = q\cdot n\cdot A\cdot D_{eff}\cdot\frac{C_0}{L} \quad (8)$$

Where the effective diffusivity is defined as:

$$\frac{1}{D_{eff}} = \frac{1}{D_{Ox}} + \frac{1}{D_R} \quad (9)$$

and C_0 is the initial concentration of the oxidant in the system:

$$C_0 = \frac{N_T}{Volume} = \frac{N_T}{A\cdot L} \quad (10)$$

The analysis of Anderson and Reilley [15] showed that the current limit of a thin electrolyte cell reaches a steady state which is inversely proportional to the distance between the electrodes, L. This is compared to a single working electrode using the conventional Cottrell's model [21,22], where the anodic current (in the case of oxidation only) decreases with time until it diminishes to zero.

2. 1D steady-state model

A model that takes into consideration all the electrochemical reaction rates at the electrode is presented here. This model can be used to describe the DC characteristics of such a device under redox cycling at both diffusion-limited conditions ("full redox cycling") and also where the electrode reaction rate is not high enough (at relatively low over-potentials) so the current is limited by both transport and surface reaction rates ("weak redox cycling").

The model of Anderson and Reilley [15] assumes a diffusion-limited device. This model could be extended to take into consideration the electrode surface reaction rates k_{ox} and k_r (Assuming a 1st-order chemical reaction) determining the species flux at the electrodes. The flux of reductant species to the anode, $F_r(L)$, (The electrode at $x = L$ with the index "2″), is given by:

$$F_r(L) = D_r\cdot\frac{[C_r(0) - C_r(L)]}{L} = k_{ox,2}\cdot C_r(L) - k_{r,2}\cdot C_{ox}(L) \quad (11)$$

While the flux of the oxidant species to the cathode, $F_{ox}(0)$ (The electrode at $x = 0$ with the index "1″) is given by:

$$F_{ox}(0) = D_{ox}\cdot\frac{[C_{ox}(L) - C_{ox}(0)]}{L} = k_{r,1}\cdot C_{ox}(0) - k_{ox,1}\cdot C_r(0) \quad (12)$$

From those expressions, we get:

$$C_r(0) = C_r(L)\cdot\left(1 + \frac{k_{ox,2}\cdot L}{D_r}\right) - \frac{k_{r,2}}{D_r}\cdot C_{ox}(L) \quad (13)$$

$$C_{ox}(L) = C_{ox}(0)\cdot\left(1 + \frac{k_{r,1}\cdot L}{D_{ox}}\right) - \frac{k_{ox,1}}{D_{ox}}\cdot C_r(0) \quad (14)$$

Since the fluxes are fixed and equal we can define a flux, $F = F_{ox}(0) = F_r(L)$ and write the following equality:

$$D_{ox}\cdot\frac{[C_{Ox}(L) - C_{Ox}(0)]}{L} = D_R\cdot\frac{[C_R(0) - C_R(L)]}{L} \rightarrow D_{ox}\cdot[C_{Ox}(L) - C_{Ox}(0)] = D_R\cdot[C_R(0) - C_R(L)] \quad (15)$$

Note that we define both fluxes as positive. Both fluxes can be written by their surface reaction rates:

$$k_{ox,2}\cdot C_r(L) - k_{r,2}\cdot C_{ox}(L) = k_{r,1}\cdot C_{ox}(0) - k_{ox,1}\cdot C_r(0) \quad (16)$$

It is assumed that the initial Oxidant concertation is, C_0, and the total initial oxidant molecule is $N_T = C_0\cdot L\cdot A$ where A is the device area cross-section and L is the distance between the electrodes. The mass conservation law is given by $N_{0x} + N_R = N_T$, where N_{0x} *and* N_R are the total number of the Oxidant and the reductant molecules, respectively; This can be written as:

$$\left[\frac{C_{ox}(0) + C_{ox}(L)}{2}\right]\cdot L\cdot A + \left[\frac{C_r(0) + C_r(L)}{2}\right]\cdot L\cdot A = C_0\cdot L\cdot A \rightarrow C_{ox}(0) + C_{ox}(L) + C_r(0) + C_r(L) = 2\cdot C_0 \quad (17)$$

Where L·A is the volume of the device (L is its length and A is its area).

To simplify the calculation, and also since this paper relates to devices where $\eta_{ox}, -\eta_r \gg \frac{kT}{q}$ we can assume that : $k_{ox,2}\cdot C_r(L) \gg k_{r,2}\cdot C_{ox}(L)$ and $k_{r,1}\cdot C_{ox}(0) \gg k_{ox,1}\cdot C_r(0)$

Using those expressions the flux F and the current I due to that flux can be found (See supplementary material, SM1):

$$F = \frac{C_0}{\frac{1}{k_{ox,2}} + \frac{1}{k_{r,1}} + \frac{L}{2}\cdot\left(\frac{1}{D_{Ox}} + \frac{1}{D_R}\right)} = \frac{C_0}{\frac{1}{k_{eff}} + \frac{L}{D_{eff}}} \rightarrow I = qnAF = \frac{qnAk_{eff}\cdot C_0}{1 + \frac{L\cdot k_{eff}}{D_{eff}}} \quad (18)$$

D_{eff} was defined in Eq. (9), and the effective reaction velocity, k_{eff}, is defined as:

$$\frac{1}{k_{eff}} \equiv \frac{1}{k_{ox,2}} + \frac{1}{k_{r,1}} \quad (19)$$

This model shows that the flux in a thin electrolyte is bound by $Flux = k_{eff}\cdot C_0$ which occurs for cell length less than the critical length L_c:

$$L < L_c = \frac{D_{eff}}{k_{eff}} \tag{20}$$

Note that the reaction coefficients, k_{ox} and k_r, depend exponentially on the overpotential of each electrode, therefore, they can vary significantly during experiments. For longer devices, the limiting flux converges to the solution presented in the paper of Anderson and Reilley [15]. Note that this model assumes that there are no side reactions causing loss of the reductants or oxidants ions.

The model that is presented here is an approximation since it assumes that at one working electrode there is only oxidation, and at the other electrode there is only reduction. This assumption leads to a result with a small non-zero current at equilibrium when the overpotentials are zero. However, this error is observable only at a very low current, when the applied overpotential is low. This error is negligible for most applications where a large overpotential is applied and only one term, with the bigger exponent, is taken in the Butler-Volmer equation. Therefore, in cases where a more accurate model is needed, for a very small current it can be done by adding the components related to the reverse current on each one of the working electrodes, i.e., adding a reduction component on the oxidizing electrode and an oxidizing term on the reducing electrode. We neglected this here on purpose to simplify the model and make it implantable onto advanced electronic circuit simulators like SPICE and using high-definition languages such as VERILOG A. This is justified in the case discussed in this paper which relates to bio-electrochemical sensors. In most bio-electrochemical sensors operating under redox cycling mode, the overpotentials are determined to allow "almost" only oxidation on one electrode and "almost" only reduction on the other.

The current in the case where the cathode is at very negative bias and the positive electrode bias is varying in such a way that $k_{eff} \sim k_{ox,0,2} \cdot e^{b_a \cdot V}$ is given by:

$$I = \frac{qnAC_0 \cdot k_{ox,0,2} \cdot e^{b_a \cdot V}}{1 + L \cdot \frac{k_{ox,0,2} \cdot e^{b_a \cdot V}}{D_{eff}}} = I_{max} \cdot \frac{a_{ox} \cdot e^{b_a \cdot V}}{1 + a_{ox} \cdot e^{b_a \cdot V}} \tag{21}$$

Where the index 2 means that it is related to the positive (right) electrode. The constants I_{max} and a_{ox} are defined as $I_{max} = \frac{qnAD_{eff}C_0}{L}$ *and* $a_{ox} = \frac{L \cdot k_{ox,0,2}}{D_{eff}}$. That expression can be written as: $\frac{I_{max}}{I} - 1 = \frac{e^{-b_a \cdot V}}{a_{ox}}$ or alternatively as: $\ln\left(\frac{I_{max}}{I} - 1\right) = -\ln(a_{ox}) - b_a \cdot V$. Note that we ignored the serial resistance (Ohmic polarization). Assuming an applied voltage V_a and serial resistance R the voltage drop on the anode is $V = V_a - IR$. This means that as the current increases the I-V plot shifts to a more positive bias and its slope decreases. In most cases of biosensors, the current is in the range of 1 nA-10 μA, and the serial resistance is in the range of a few 100 Ohms, therefore the IR drop is below a few mVs, hence it is negligible.

3. Small signal modeling

In this section, the small signal impedance model of the two-working electrode device operating under redox cycling conditions is presented. Similar solutions to other devices exist in numerous papers, for example: Lasia et al. [23], Sluyters-Rehbach [24], Vivier and Orazem [25], and Diard et al. [26].

First, we will calculate the derivative of the current vs. voltage of the device under redox cycling conditions. It is assumed that a small signal is applied to the oxidizing electrode while the other electrode is at a fixed bias. Therefore, the reaction coefficients are: $k_{ox} = \overline{k}_{ox} + dk_{ox}$ and $k_R = \overline{k}_R$ where the notation $\overline{k}$ refers to steady state condition of the variable k and dk is the change in k due to a small signal excitation. Using this notation, we find the small signal admittance of the device under redox-cycling condition, neglecting diffusion effects, is given by:

$$g_{rc} \equiv \frac{\partial I}{\partial V} = I_{max} \cdot \frac{a_{ox} \cdot b_a e^{b_a \cdot V}}{(1 + a_{ox} \cdot e^{b_a \cdot V})^2} \tag{22}$$

This function has a maximum where $a_{ox} \cdot e^{b_a \cdot V} = 1$ and its maximum value is $g_{rc,m} = \frac{I_{max} \cdot b_a}{4}$.

Next, we calculate the response of the device to sinusoidal excitation:

$$V(t) = \overline{V} + \widetilde{v} \cdot e^{j\omega t} \tag{23}$$

This will result in small signal variations in the concentration of the reductant and oxidant species $C(t) = \overline{C} + \widetilde{c} \cdot e^{j\omega t}$ and will result in sinusoidal fluctuations in the current $I(t) = \overline{I} + \widetilde{i} \cdot e^{j\omega t}$. $\overline{V,C,}$ *and* $\overline{I,}$ are the steady state (DC) values of the voltage, concentration, and current while $\widetilde{v}$, $\widetilde{c}$ *and* $\widetilde{i}$ are the phasors of those variables, respectively.

The fluctuations in the concentration of the reductant and oxidant in response to sinusoidal excitation can be solved using the diffusion equations:

$$\frac{\partial C_{ox}}{\partial t} = D_{Ox} \cdot \frac{\partial^2 C_{ox}}{\partial x^2} \rightarrow j\omega \widetilde{c}_{ox} = D_{ox} \cdot \frac{d^2 \widetilde{c}_{ox}}{dx^2} \rightarrow \frac{d^2 \widetilde{c}_{ox}}{dx^2} - \frac{\widetilde{c}_{ox}}{L_{D,ox}^2} = 0 \tag{24}$$

$$\frac{\partial C_r}{\partial t} = D_r \cdot \frac{\partial^2 C_r}{\partial x^2} \rightarrow j\omega \widetilde{c}_r = D_r \cdot \frac{d^2 \widetilde{c}_r}{dx^2} \rightarrow \frac{d^2 \widetilde{c}_r}{dx^2} - \frac{\widetilde{c}_r}{L_{D,r}^2} = 0 \tag{25}$$

Where the complex diffusion length is given by:

$$L_{D,Ox}^2 = \frac{D_{Ox}}{j\omega} \;\&\; L_{D,R}^2 = \frac{D_R}{j\omega} \tag{26}$$

The solution for this set of equations under the boundary conditions of the device with two working electrodes where the AC bias is applied to the positive electrode yields the following expression for Warburg impedance (See supplementary material, SM2):

$$Z(\omega) = \frac{L}{qnAD_r \cdot \frac{q\alpha}{nkT} \cdot \overline{C}_r} \cdot h(\omega) = \frac{nkT}{q\alpha} \cdot \frac{1}{I_{DC}} \cdot h(\omega) \tag{27}$$

Where the function h is given by:

$$h(\omega) \equiv \frac{\left(\frac{L_{D,R}}{L}\right)}{\sinh\left(\frac{L}{L_{D,R}}\right)} \cdot \left\{ \left[\cosh\left(\frac{L}{L_{D,R}}\right) + \frac{D_r}{\overline{K}_{ox,2} \cdot L_{D,R}} \cdot \sinh\left(\frac{L}{L_{D,R}}\right) \right] - \frac{1}{\left[\cosh\left(\frac{L}{L_{D,Ox}}\right) + \frac{D_{ox}}{\overline{K}_{r,1} \cdot L_{D,Ox}} \cdot \sinh\left(\frac{L}{L_{D,Ox}}\right) \right]} \right\} \tag{28}$$

Where ω is the angular frequency that is defined as: $\omega = 2\pi f$ where f is the frequency of the ac signal. $\overline{K}_{ox,2}$ is the DC oxidation reaction coefficient at the anode, $\overline{K}_{r,1}$ is the DC reduction reaction coefficient at the cathode, D_{ox} *and* $L_{D,Ox} = \sqrt{D_{ox}/j\omega}$ are the diffusivity and the complex diffusion length of the oxidant species, D_r *and* $L_{D,r} = \sqrt{D_r/j\omega}$ are the diffusivity and the complex diffusion length of the reductant species and L is the spacing between the two working electrodes.

Here is a brief exploration of the function $h(\omega)$ for p-nitrophenol

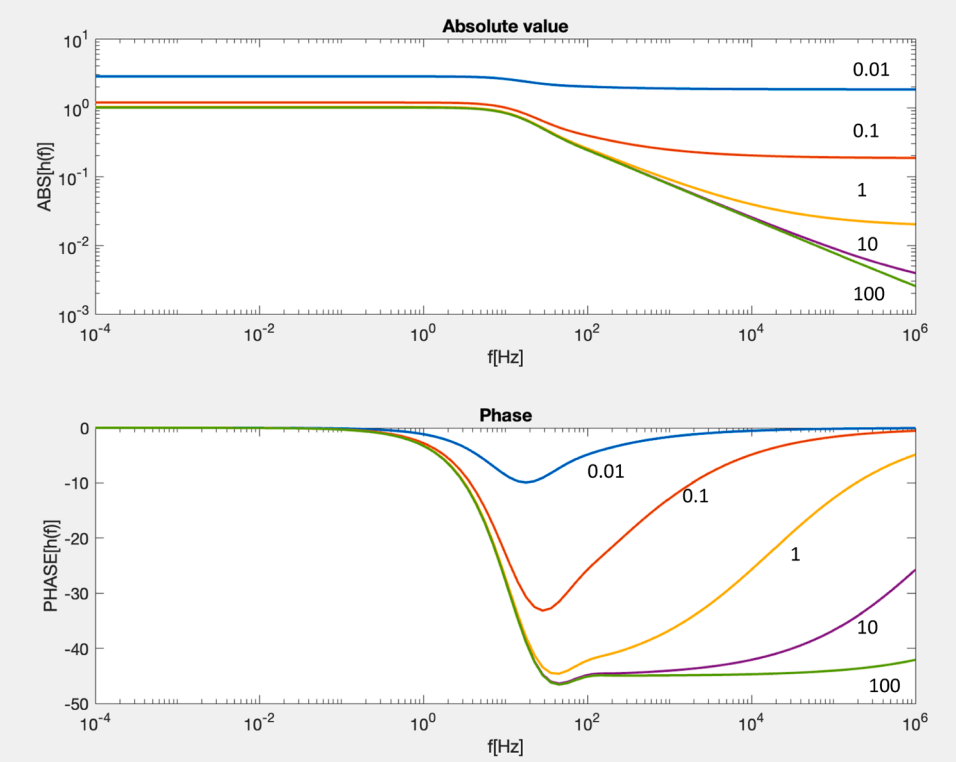


Fig. 2. The absolute value and phase of h(f) (Eq. (28)) for K_{ox} =0.01,0.1,1,10 and 100 cm/sec when K_r=100 cm/sec. (D_r=D_{ox}=9.2 × 10^{-6} cm/sec, L = 5 μm).

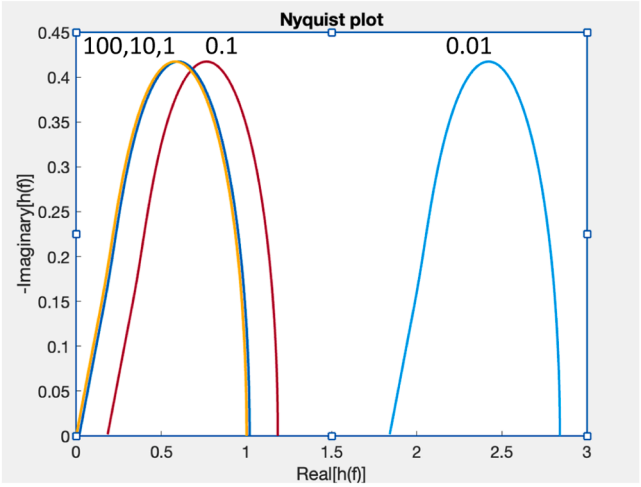


Fig. 3. Nyquist plot of h(f) (Eq. (28)) for Kr=100 cm/sec and K_{ox} varies in the range of 0.01 to 100 cm/sec, (D_r=D_{ox}=9.2 × 10^{-6} cm^2/sec, L = 5 μm).

(PNP) which is a common product in a few useful bio-electrochemical sensors [14]. PNP diffusivity in aqueous solutions is about 0.92×10^{-5} cm^2/sec [32]. Let's assume the same diffusivity for both the oxidant and reductant states of p-Nitrophenol during the redox-cycling situation. First, a short exploration is presented regarding the effect of the oxidation reaction coefficient (K_{ox}) on the positive electrode (where the ac excitation is applied) for a device with a 5-micron space between the two working electrodes. Redox oxidation becomes significant when the oxidation rate is significantly large (Eq. (18)): $K_{eff} > D_{eff}/L$ or $K_{ox} > D_{ox}/2L$. Hence for $L = 5$ μm, we get that the redox cycling becomes dominant when $K_{ox} > 0.92\times10^{-2}$ cm/sec. Therefore, the simulation was done for $K_{ox} = 10^{-2}$, 10^{-1},1,10, and 10^{2} cm/*sec* while the reduction rate coefficient at the fixed bias electrode was kept fixed at $K_r = 10^2$ cm/sec. (Fig. 2, Bode plot and Fig. 3, Nyquist plot). The dependence of the functon h (Eqn 28) on the reduction rate of the non-excited working electrode, where there is only DC bisa and the oxidation rate on the ac-excited electrode is 100 cm/sec, is shown in Fig. 4 (Bode plot) and Fig. 5 (Nyquist plot).

The frequency response depends also on the space between the two working electrodes. As the distance shrinks the cutoff frequency, where the impedance drops by 3 dB is shifting to a higher frequency. An interesting effect is observed on the Nyquist plot (Fig. 6) for spacing in the range of < 0.1 μm (for D_r=D_{ox}=9.2 × 10^{-6} cm^2/sec) under redox cycling conditions where K_{ox} & K_r are high enough.

Under redox cycling conditions, the reaction rates, K_{ox} and K_r are high enough and we see that there is no effect of the shape of the frequency dependence of the impedance. Under this regime of operation, we can provide an approximation for h(f). The function h can be written also as:

$$h(X_r) \equiv \frac{1}{X_r \cdot sinh(X_r)} \cdot \left\{ [cosh(X_r) + \beta_r \cdot sinh(X_r)] - \frac{1}{[cosh(X_{ox}) + \beta_{ox} \cdot sinh(X_{ox})]} \right\} \quad (29)$$

Where $\beta_r = \frac{D_r}{\overline{K}_{ox,2} \cdot L_{D,R}} = \frac{\sqrt{j \cdot D_r \cdot \omega}}{\overline{K}_{ox,2}}$, $\beta_{ox} = \frac{D_{ox}}{\overline{K}_{r,1} \cdot L_{D,ox}} = \frac{\sqrt{j \cdot D_{ox} \cdot \omega}}{\overline{K}_{r,1}}$. and:

$$X_r \equiv \frac{L}{L_{D,R}} = (j \cdot \theta_r)^{\frac{1}{2}} \text{ and } \theta_r = \frac{\omega \cdot L^2}{D_r} = \omega \cdot \tau_{D,r} \text{ where } \tau_{D,r} = \frac{L^2}{D_r} \quad (30)$$

$$X_{ox} \equiv \frac{L}{L_{D,ox}} = (j \cdot \theta_{ox})^{\frac{1}{2}} \text{ and } \theta_{ox} = \frac{\omega \cdot L^2}{D_{ox}} = \omega \cdot \tau_{D,ox} \text{ where } \tau_{D,ox} = \frac{L^2}{D_{ox}} \quad (31)$$

Note that the impedance depends on four unitless factors: β_r, β_{ox}, X_r, *and* X_{ox}. All of them depend on the diffusion length which is a complex number with a value that is proportional to the square root of the frequency and a phase of 45° The absolute values of the hyperbolic sinus terms with β_r& β_{ox} are small when the angular frequency is $\omega < \frac{(\overline{k}_{ox,2})^2}{D_r}$, $\frac{(\overline{k}_{r,1})^2}{D_{ox}}$. In that frequency range, if we assume $L_{D,R} \approx L_{D,Ox} = L_D$ we get the following approximation:

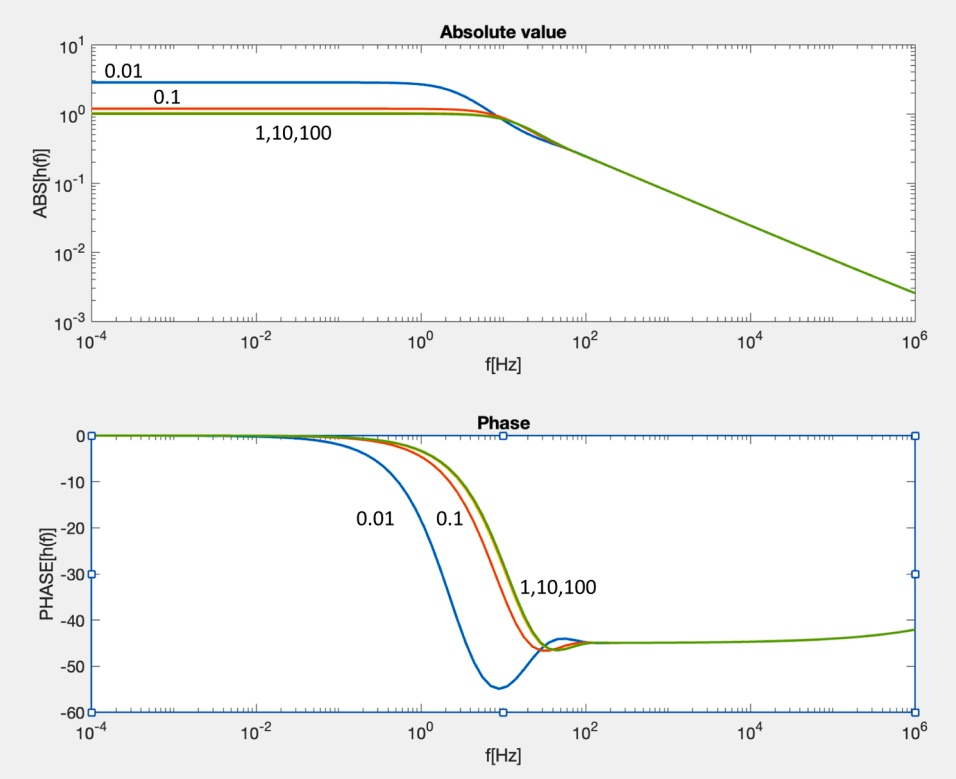


Fig. 4. The absolute value and phase of h(f) (Eq. (28)) for K_r =0.0001,0.001,0.01,0.1,1,10 and 100 cm/sec when K_{ox}=100 cm/sec. (D_r=D_{ox}=9.2 × 10^{-6} cm^2/sec, L = 5 μm).

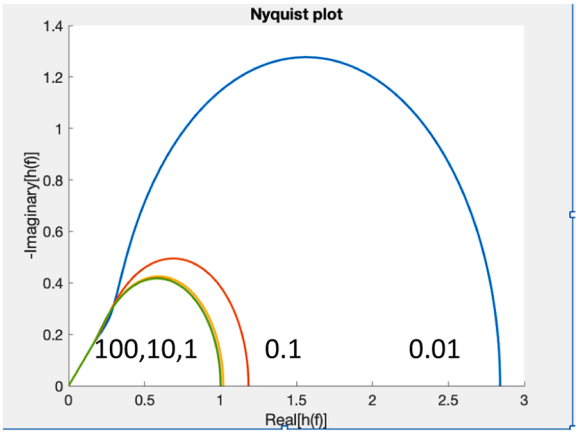


Fig. 5. Nyquist plot of h(f) (Eq. (28)) for K_{ox}=100 cm/*sec* and K_r varies in the range of 0.01 to 100 cm/sec, (D_r=D_{ox}=9.2 × 10^{-6} cm^2/sec, L = 5 μm).

$$h(X_r) \approx \frac{[cosh(X_r)\,]^2 - 1}{X_r \cdot sinh(X_r)} = \frac{tanh(X_r)}{X_r} = \frac{\tanh\left[(j\cdot\theta_r)^{\frac{1}{2}}\right]}{(j\cdot\theta_r)^{\frac{1}{2}}} \rightarrow h(f)$$
$$= \frac{\tanh\left[\sqrt{j\cdot\frac{2\pi f\cdot L^2}{D_r}}\right]}{\sqrt{j\cdot\frac{2\pi f\cdot L^2}{D_r}}} \qquad (32)$$

the function, $h(X_r)$ is shown vs the normalized parameter θ_r in Fig. 7.

The maximum of the Nyquist plot (Fig. 8) occurs where $\theta_{max} \approx 2.54$. The value of h(f) at that frequency is: 0.5817 - 0.4172i (in polar coordinates: $0.7158\angle - 35.65^o$). Converting θ_{max} to frequency, we get $f_{max} \approx 0.4/\tau_D = (0.4\cdot D_{ox}/L^2)$. Hence, as the inter-electrode spacing dimension shrinks, that frequency increases.

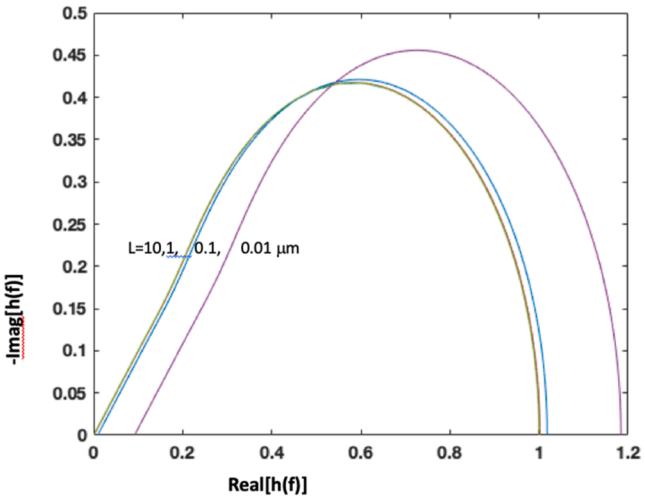


Fig. 6. : the Nyquist plot for various distances between the two working electrodes (D_r=D_{ox}=9.2 × 10^{-6} cm^2/sec).

4. Experimental

To demonstrate the Electrochemical Impedance Spectroscopy under redox cycling conditions we present here both experimental results, using an interdigitated electrode array (IDA) implemented in a microfluidic device, and the results of a 3D simulation of the same device.

The experimental results were obtained using interdigitated (gold) electrode array chips, purchased from Microx® Technologies. The chips under study were selected to have the same effective area for both generator and collector electrodes (Table 1).

The chips are composed of four electrodes: two working electrodes, a

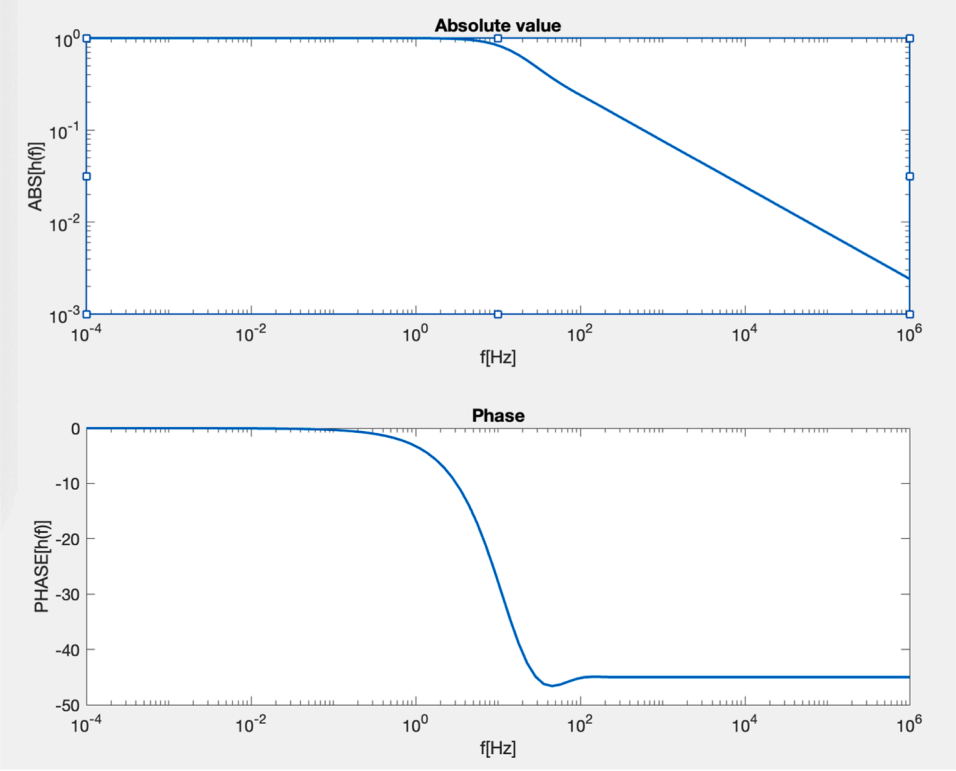


Fig. 7. The amplitude and phase of the function $h(f)$, (Eq. (32)), as a function of the frequency.

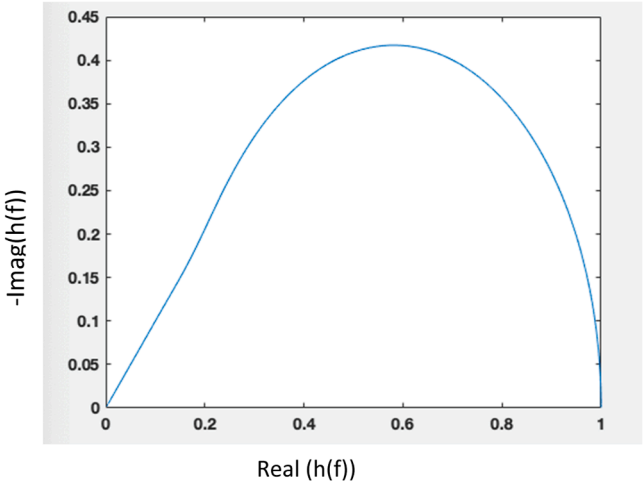


Fig. 8. Nyquist plot of the normalized impedance function, see (Eq. (32)).

Table 1
MicruX® Technologies interdigitated electrode array parameters (Single electrode length = 1640 μm).

	IDA1-Au	IDA6-Au
The gap between WEs [μm]	10	5
WEs' width [μm]	10	5
WEs' height [μm]	0.15	0.15
Number of WEs pairs	15	30
Generator/collector area [cm^2]	2.46E-03	2.46E-03

reference, and an auxiliary. The working electrodes are structured in a comb shape, with equal spacing and widths, of 5 and 10 μm. For each generator/collector electrode, the total length (of all the fingers that are exposed to the electrolyte) is 1.64 mm. Finally, the quasi-reference Ag/AgCl electrode was prepared by silver electroplating from a standard nitrate bath followed by anodization in HCl 0.1 M. The materials were purchased from Sigma Aldrich Inc. All measurements were repeated three to four times, and the average value was used for data analysis.

The electrochemical characterization was performed using a Palmmsens-4® bi-potentiostat. The cyclic voltammetry (CV) was obtained for 6 mM ferricyanide [$K_3Fe(CN)_6$] in 0.1 M PBS, pH 7.4 solution, where the first working electrode's potential was scanned between −0.8 V and 1 V at a 100 mV/ sec scan rate, and the second was biased with a constant 1 V potential. Three potential scans were performed for each measurement and the data was captured from the second scan. For the electrochemical impedance spectroscopy (EIS) measurements, 10 mM and 100 mM ferricyanide in 0.1 M KNO_3 were used and the details of the scan conditions appear in the "Impedance" section. The simulation model was designed to study the electrochemical behavior of a ferricyanide sensor with an interdigitated electrode array. The model was built using COMSOL Multiphysics 5.5 with an electrochemistry module, as described in detail in a previous publication [28].

5. DC characteristics

We present here two types of results; both are related to the device under test which is described in the next figure. We present here the experimental result of a real device and the results of its simulation using COMSOL. The system was characterized for a 6 mM ferricyanide [$K_3Fe(CN)_6$] in PBS buffer, as a function of the first working electrode while the second working electrode was kept at +1 V. Hence, the system is under full redox cycling below about −0.3 V, in the interim weak redox cycling mode in the range of −300 mV to ~100 mV and without redox cycling above ~ 100 mV. We present the cyclic voltammetry results that were measured in the experimental setup at 5 and 10 μm distances between the first and second working electrodes. Additionally, we created a model that simulates the electrochemical behavior at various distances of 0.5, 1, 2, 3, and 10 μm. As expected, the current at the redox-cycling regime is inversely proportional to the distance between the working electrodes.

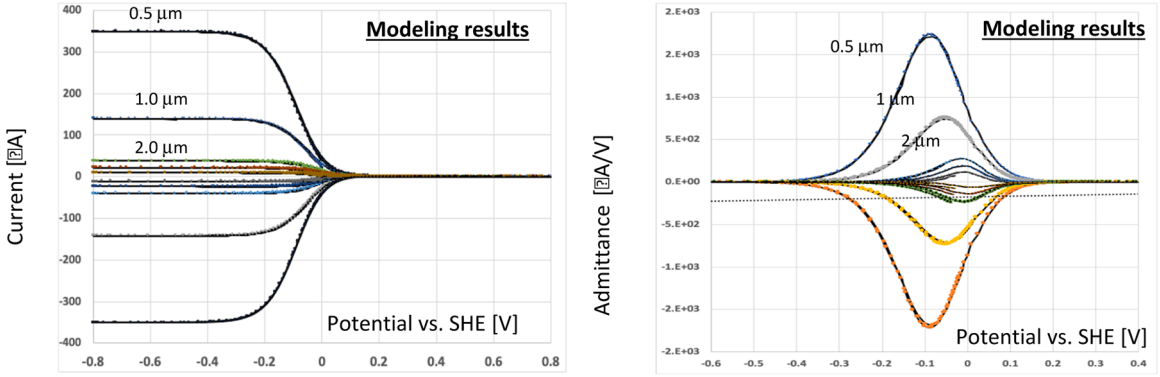


Fig. 9. Current vs. potential characteristics (left) and its derivative (right) for redox cycling in an IDA with 0.5, 1, 2, 3, & 10 µm space, obtained from 3D COMSOL Multiphysics® computational simulations.

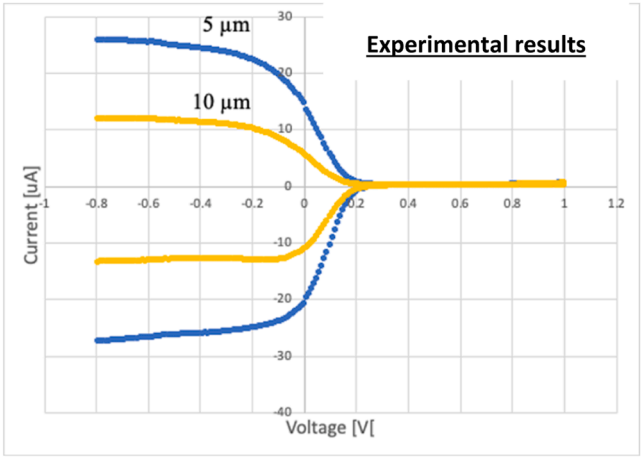


Fig. 10. Current vs. voltage characteristics for redox cycling in an IDA with 5, & 10 µm space vs. Ag/ AgCl quasi reference electrode, obtained from experimental results.

We show both the theoretical modeling using COMSOL Multiphysics (Fig. 9) and experimental results of an Interdigitated Electrode Array (IDA) with identical dimensions to that of the simulation (Fig. 10). There is a slight shift of about 150–200 mV between the simulated IV characteristics to the measured one. It is because in "real life" we use an Ag/AgCl quasi-reference electrode while the simulation was performed where the potential is assumed to be calibrated vs. a Standard Hydrogen Electrode (SHE). Other than that, the simulation fits nicely the data.

According to the model, the admittance, that was defined as $g_{rc} \equiv \partial I / \partial V$, reaches a peak at the transition region between no-redox cycling to full redox cycling. Therefore, the impedance, which is $1/g_{rc}$, reaches a minimum that depends on the distance between the electrodes (Eq. (22)).

6. Impedance

The electrochemical Impedance spectroscopy was measured in three bias points of the 1st working electrode (W1) while the bias of the other working electrode (W2) was kept at +1V:

- Strong (full) redox cycling: $V_{W1} = -0.3$ V
- Weak (partial) redox cycling: $V_{W1} = -0.05$ V for the 10 µm electrodes and $V_{W1} = -0.1$ V for the 5 µm electrode. (The slight difference in bias voltage was administered to compensate for a small lateral shift between the experiments due to experimental variations)
- No redox cycling: $V_{W1} = +0.5$ V.

Therefore, the dual-electrode system was measured at full redox cycling mode, weak redox cycling, and no redox cycling, respectively. The aqueous electrolyte included 10 mM ferricyanide ($K_3Fe(CN)_6$) in 100 mM KNO_3. We present both the Bodé plots (Fig. 11) and the Nyquist plots of the measurements. (Fig. 12).

The measurements presented in Figs. 11 and 12 show the results for the three regimes. First, we analyze the Bodé plots. Without redox cycling the impedance was capacitive for almost 5 orders of magnitudes: from 0.1 Hz to 10 KHz. Above 10 KHz all the impedance measurements converged to the serial resistance which was in the range of slightly above 100 Ohms. It was also found that the low-frequency impedance is increasing as the redox cycling increases. It was also observed that the absolute value of the phase at low frequency is much higher than −45°, and closer to 0°. This is predicted by our model which anticipates a more resistive behavior at low frequency than for the case of a single electrode system which is typically characterized using the Warburg impedance.

The Nyquist plot shows the same data and shows that the impedance at full redox cycling is much higher than that at weak redox cycling. The Nyquist plot with full redox cycling has two regimes. At high and intermediate frequencies, it is a half-circle, as expected from the effect of the charge transfer impedance in parallel to the double-layer capacitance. However, at lower frequencies, the Nyquist plot of devices under strong redox cycling does not increase at a 45 slope as predicted by the Warburg model. Especially for the 5 µm spacing electrodes, where the redox cycling is more pronounced the Nyquist plot at the low-frequency regime differs significantly from the classical Warburg model and looks more like a semicircle as predicted by the model developed in this work. However, that observation must be critically examined since the proposed model is only for one effect, the diffusion-related impedance, while the real device impedance is affected also by other effects such as the double layer capacitance and the serial resistance of the solution, wires, and contacts.

The impedance of the same electrodes was explored for two different KNO_3 concentrations (Fig. 13).

The left side of the Nyquist plots in Fig. 13 can be approximately modeled using a simple equivalent network with a serial resistance, R_s, connected in series to a capacitor, C_p, that is connected in parallel to a resistor, R_p [27]In this model, the impedance is $R_s + \frac{R_p}{1+j\omega R_p C_p}$ A slightly better fitting is achieved by assuming that the impedance is modeled by: $R_s + \frac{R_p}{\left[1+\left(j\omega R_p C_p\right)^p\right]^{1/p}}$ where p was assumed to be in the range of 0.8–0.9. The values of the frequency at the maximum of the semi-circle and the lumped components values are shown in Table 2. Note that the error in the estimated value is rather high, > 10 %.

7. Discussion & conclusions

In his work, we present DC and AC models for a 1D four-electrode

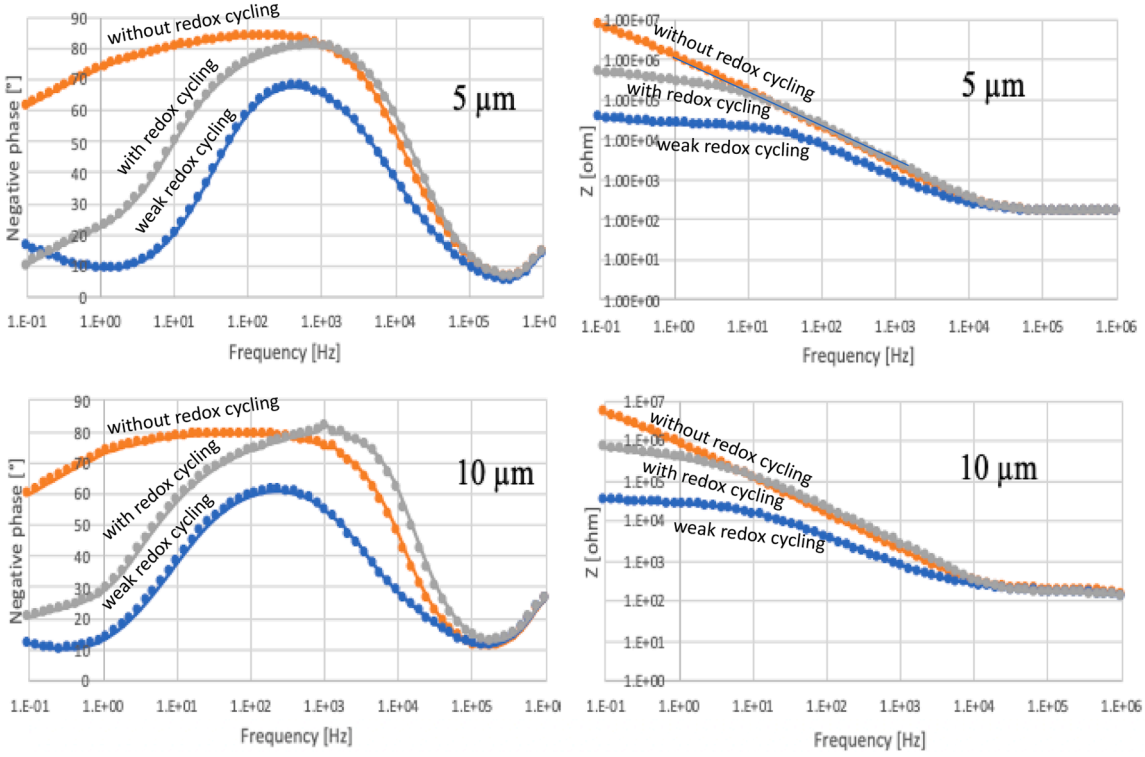


Fig. 11. Bodé plots of the EIS of 10 mM ferricyanide ($K_3Fe(CN)_6$) in 100 mM KNO_3, without redox cycling (orange), with weak redox cycling (blue), and under complete redox cycling conditions (gray).

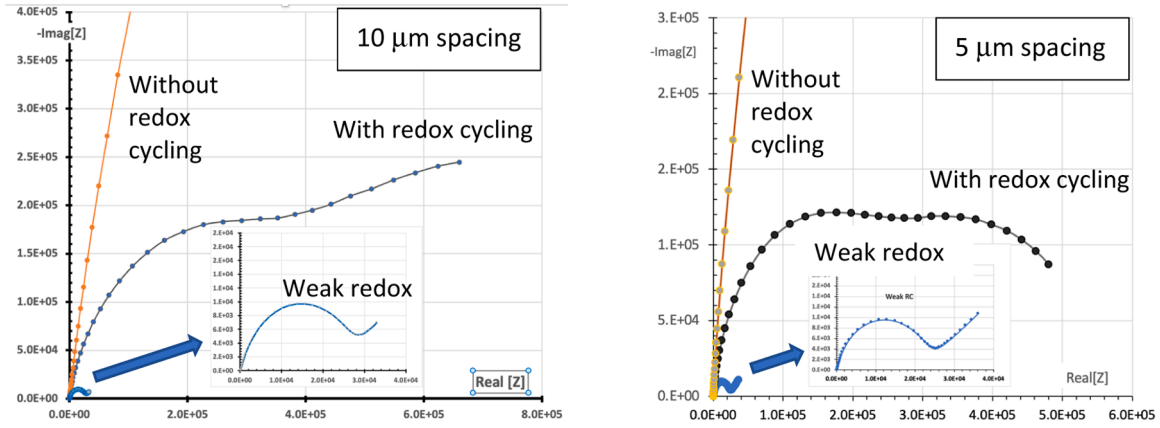


Fig. 12. Nyquist plot of the EIS of 10 mM ferricyanide ($K_3Fe(CN)_6$) in 100 mM KNO_3, (Left), (right) 5 µm spacing).

electrochemical cell and experimental results for an interdigitated electrode array. The results indicated that there are three regimes of operation: 1. No redox cycling, 2. Transition region (weak cycling) and 3. Full redox cycling. Full redox cycling occurs when the reaction rates at both working electrodes exceed a critical value of approximately $k > D/L$. (her k refers to both anodic and cathodic reaction rates, D is the active species diffusivity and L the distance between the two working electrodes). Since the diffusivity of the species in our experiment is in the range of 10^{-5} cm^2/sec [32] and the distance between the electrodes is 5–10 µm the critical reaction rates to achieve full redox cycling should significantly exceed $\sim 10^{-2}$ cm/sec.

The impedance results indicated that when there is no redox cycling, the dominant component that affects the impedance is the double-layer capacitance. In that case, the impedance is mostly capacitive, it is inversely proportional to the frequency and the phase is close to $-90°$ for almost 3 orders of magnitudes. All the measured Bodé plots converge at high frequency to the residual resistance at high frequency which is in the range of ~100 Ohms. That serial resistance is mostly attributed to the gold electrode array wire resistance. Each finger out of the 15 fingers in the interdigitated electrode array, has a resistance of a few Ohms. Other sources for that serial resistance are the contacts and the external wire-to-contact interface.

Under redox cycling, in both weak and strong conditions, there is a significant reduction of the imaginary part of the impedance at low frequencies. The effect also depends on the spacing between the electrodes. As predicted by the model, the low-frequency impedance at the transition region (V~0.05 V) is less than that at the "full" redox cycling regime ($V = 0.5$ V). This effect is noticeable for both solutions with 100 mM and 10 mM "Ferri/Ferro" compounds [29]. The measurements were limited to above 100 mHz and did not reveal the full extent of the transport effects on the impedance at lower frequencies.

Finally, a few comments regarding the validity of the model

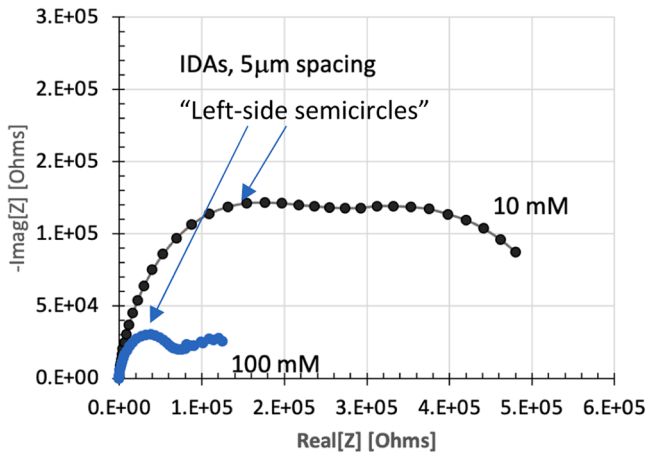


Fig. 13. Nyquist plot of the EIS of 10 mM (Top) & 100 mM (Bottom) ferricyanide ($K_3Fe(CN)_6$) in 100 mM KNO_3, for IDAs with 5 µm spacing under redox cycling conditions ($V_{gen} = -0.5$ V, $V_{collector} = 1$ V).

Table 2
The parameters of the equivalent circuit that fits the "left-side semicircle" of the Nyquist plot of the IDA with 5 µm spacing (Fig. 13). (Area = 2.46E-3 cm^2, Table 1).

Concentration [mM]	f_{peak} [Hz]	R_s [Ohm]	Rp [KOhm]	Cp [F]	Cp [F/cm^2]*
10	3.9	170±10	280±30	1.45E-7	5.9E-5
100	16.9	60±10	70±10	1.34E-7	5.4E-5

* the capacitance per unit area was calculated as the measured capacitance divided by electrode area. However, it is an interdigitated device with significant fringing fields, hence this result is a rough approximation.

presented here for real interdigitated electrodes. The model that is presented here is one-dimensional. However, interdigitated electrodes are long and narrow with a three-dimensional geometry that can be described with cylindrical symmetry for each electrode. This may affect the device characteristics since transport effects, which are dominant for interdigitated electrodes operating under redox-cycling conditions, may affect the functional behavior of 1D, 2D, and 3D systems [30,31].

The experimental DC results and the 3D models yielded similar behavior to that of the 1D model, showing that the 1D may be useful for qualitative DC analysis. For devices longer than a critical length L_c, (see Eq. (18)), the limiting flux converges to the solution presented in the paper of Anderson and Reilley [15]. That critical length depends on the redox species diffusivity and the surface reaction velocity that depends on the electrodes' overpotential. Note that this model assumes that no other side reactions are causing the loss of reductants or oxidant ions.

The model that we present here aims only to the case where there is redox-cycling and the system is not in equilibrium, although it can be in steady state. It assumes that at one working electrode, there is only oxidation, and at the other electrode there is only reeducation. This assumption leads to a small non-zero current at equilibrium when the overpotentials are zero, which is an error. However, first, this error current is small compared to the currents in the redox cycling regime this it can be neglected. Second, this error can be corrected by adding a reducing current, like in the derivation of the Butler-Volmer model. That effect on the model that is presented in this paper is observable only at a very low current, when the applied overpotential, on one of the working electrodes, is low. This is negligible for most applications where a large overpotential is applied and only one term, with the bigger exponent, is assumed dominant in the Butler-Volmer equation. Therefore, in cases where a more accurate model is needed, for a very small current it can be done by adding the components related to the reverse current on each one of the working electrodes, i.e., adding a reduction component on the oxidizing electrode and an oxidizing term on the reducing electrode. We neglected this on purpose to simplify the model and make it implantable onto advanced electronic circuit simulators like SPICE and using high-definition languages such as VERILOG A. The impedance measurements also showed qualitative behaviors like that of the 1D model. Hence, we can propose that the 1D model provides a useful explanation for the various phenomena observed even for real structures with higher-dimension structures.

CRediT authorship contribution statement

Tali Dotan: Conceptualization, Data curation, Formal analysis, Investigation, Methodology, Software, Validation, Visualization, Writing – original draft, Writing – review & editing. **Aakash Jog:** Data curation, Software, Validation. **Yosi Shacham-Diamand:** Conceptualization, Data curation, Formal analysis, Funding acquisition, Investigation, Methodology, Project administration, Resources, Software, Supervision, Validation, Visualization, Writing – original draft, Writing – review & editing.

Declaration of competing interest

The authors declare the following financial interests/personal relationships which may be considered as potential competing interests:

Y. Shacham-Diamand reports financial support was provided by Israel Science Foundation. Y. Shacham-Diamand reports financial support was provided by Israel Ministry of Innovation Science & Technology. Tali Dotan reports financial support was provided by Manna Centre for Food Security, Tel Aviv University.

Data availability

Data will be made available on request.

Acknowledgments

First, thanks to our colleagues who helped us in this research. Thanks to Prof. Marc Madou from UCI whom we started with our research a few years ago and shared many ideas. His suggestions and help at the beginning of this research are highly appreciated. We also thank Dr. Antonio Valletta from the CNR-IMM, Rome, Italy for his valuable help with the COMSOL® modeling.

Next, thanks to our support. The research was partially funded by the Israel Innovation Authority (IIA) "Biochip" consortium, the Israel Science Foundation administered by the Israel Academy of Science and Humanities grant number 1616/17, the Ministry of Science and Technology grant number 01030360, and the Boris Mints Institute for Strategic Policy Solutions to Global Challenges, the Department of Public Policy, and the Manna Centre for Food Security, Tel Aviv University grant number 590351. Dr. Dotan would like to acknowledge the Ministry of Science and Technology STEM fellowship.

Finally, thanks to the Scojen Institute for Synthetic Biology, Reichman University for its generous support of this research.

Supplementary materials

Supplementary material associated with this article can be found, in the online version, at doi:10.1016/j.electacta.2024.144675.

References

[1] L. Nyholm, Electrochemical techniques for lab-on-a-chip applications, Analyst 130 (5) (2005) 599–605.

[2] N.J. Ronkainen, H.B. Halsall, W.R. Heineman, Electrochemical biosensors, Chem. Soc. Rev. 39 (5) (2010) 1747–1763.
[3] J.L. Hammond, N. Formisano, P. Estrela, S. Carrara, J. Tkac, Electrochemical biosensors and nanobiosensors, Essays Biochem. 60 (1) (2016) 69–80.
[4] E. Kätelhön, B. Wolfrum, On-chip redox cycling techniques for electrochemical detection, Rev. Anal. Chem. 31 (1) (2012) 7–14.
[5] F. Lucarelli, S. Tombelli, M. Minunni, G. Marrazza, M. Mascini, Electrochemical and piezoelectric DNA biosensors for hybridisation detection, Anal. Chim. Acta 609 (2) (2008) 139–159.
[6] I.H. Cho, J. Lee, J. Kim, M.S. Kang, J.K. Paik, S. Ku, H.M. Cho, J. Irudayaraj, D. H. Kim, Current technologies of electrochemical immunosensors: perspective on signal amplification, Sensors 18 (1) (2018) 207.
[7] S. Sharma, Microstructural Tuning of Glassy Carbon For Electrical and Electrochemical Sensor Applications, University of California, Irvine, 2013.
[8] R.R. Kamath, M.J. Madou, Three dimensional carbon interdigitated electrode arrays for redox-amplification, Anal. Chem. 86 (6) (2014) 2963–2971.
[9] R. Kamath, M.J. Madou, Selective detection of dopamine against ascorbic acid interference using 3D carbon interdigitated electrode arrays, ECS Trans. 61 (7) (2014) 65.
[10] M. Bauer, J. Bartoli, S.O. Martinez-Chapa, M. Madou, Wireless electrochemical detection on a microfluidic compact disc (CD) and evaluation of redox-amplification during flow, Micromachines. (Basel) 10 (1) (2019) 31.
[11] E. Kosri, F. Ibrahim, A. Thiha, M. Madou, Micro and nano interdigitated electrode array (IDEA)-based MEMS/NEMS as electrochemical transducers: a review, Nanomaterials 12 (23) (2022) 4171.
[12] S. Smith, D. Mager, A. Perebikovsky, E. Shamloo, D. Kinahan, R. Mishra, S. M. Torres Delgado, H. Kido, S. Saha, J. Ducrée, M. Madou, CD-based microfluidics for primary care in extreme point-of-care settings, Micromachines. (Basel) 7 (2) (2016) 22.
[13] Y. Yang, Y.Y. Yu, Y.T. Shi, J.M. Moradian, Y.C. Yong, In vivo two-way redox cycling system for independent duplexed electrochemical signal amplification, Anal. Chem. 91 (8) (2019) 4939–4942.
[14] T. Dotan, A. Jog, K. Kadan-Jamal, A. Avni, Y. Shacham-Diamand, In vivo plant bio-electrochemical sensor using redox cycling, Biosensors 13 (2) (2023) 219.
[15] L.B. Anderson, C.N. Reilley, Thin-layer electrochemistry: steady-state methods of studying rate processes, J. Electroanal. Chem. 10 (5–6) (1965) 538–552.
[16] C.R. Christensen, F.C. Anson, Chronopotentiometry in thin layers of solution, Anal. Chem. 35 (2) (1963) 205–209. Jan.
[17] C.R. Christensen, F.C. Anson, Application of thin layer chronopotentiometry to kinetic studies, Anal. Chem. 36 (3) (1964) 495–497. Mar.
[18] A.T. Hubbard, F.C. Anson, New electrodes for chronopotentiometry in thin layers of solution, Anal. Chem. 36 (4) (1964) 723–726. Apr.
[19] D.M. Oglesby, S.H. Omang, C.N. Reilley, Thin layer electrochemical studies using controlled potential or controlled current, Anal. Chem. 37 (11) (1965) 1312–1316. Oct.
[20] A.J.B. Larry, R. Faulkner, Electrochemical methods fundamentals and applications, vol. 2. 2012.
[21] F.G. Cottrell, Residual current in galvanic polarization, regarded as a diffusion problem, Z. Phys. Chem. 42 (1903) 385–431.
[22] F.G. Cottrell, Application of the Cottrell equation to chronoamperometry, Z Phys. Chem. 42 (1902) 385.
[23] A. Lasia, D. Grégoire, General model of electrochemical hydrogen absorption into metals, J. Electrochem. Soc. 142 (10) (1995) 3393–3399.
[24] M. Sluyters-Rehbach, Impedances of electrochemical systems: terminology, nomenclature and representation part I: cells with metal electrodes and liquid solutions, Pure Appl. Chem. 66 (9) (1994) 1831–1891.
[25] V. Vivier, M.E. Orazem, Impedance analysis of electrochemical systems, Chem. Rev. 122 (12) (2022) 11131–11168.
[26] J.P. Diard, B. Le Gorrec, C. Montella. Handbook of electrochemical impedance spectroscopy, 2008.
[27] J.E.B. Randles, Kinetics of rapid electrode reactions, Faraday Discuss. 1 (1947) 11–19.
[28] T. Dotan, M. Nazarenko, Y. Atiya, Y. Shacham-Diamand, Transport effects in biochip sensors with redox cycling amplification, Electrochim. Acta 459 (2023) 142520. Aug.
[29] H. Saraç, M.A. Patrick, A.A. Wragg, Physical properties of the ternary electrolyte potassium ferri-ferrocyanide in aqueous sodium hydroxide solution in the range 10-90°C, J. Appl. Electrochem. 23 (1) (1993) 51–55.
[30] H.R. Zafarani, K. Mathwig, E.J. Sudhölter, L. Rassaei, Electrochemical redox cycling in a new nanogap sensor: design and simulation, J. Electroanal. Chem. 760 (2016) 42–47.
[31] C. Amatore, C. Sella, L. Thouin, Electrochemical time-of-flight responses at double-band generator-collector devices under pulsed conditions, J. Electroanal. Chem. 593 (1–2) (2006) 194–202.
[32] R. Niesner, A. Heintz, Diffusion coefficients of aromatics in aqueous solution, J. Chem. Eng. Data 45 (6) (2000) 1121–1124.